PAPER

Ground- and excited-state scattering potentials for the stopping of protons in an electron gas

IOP Publishing Journal of Physics B: Atomic, Molecular and Optical Physics
J. Phys. B: At. Mol. Opt. Phys. **50** (2017) 185201 (8pp) https://doi.org/10.1088/1361-6455/aa843d

Ground- and excited-state scattering potentials for the stopping of protons in an electron gas

F Matias[1], R C Fadanelli[1], P L Grande[1], N E Koval[2], R Díez Muiño[3], A G Borisov[4], N R Arista[5] and G Schiwietz[6]

[1] Ion Implantation Laboratory, Instituto de Física, Universidade Federal do Rio Grande do Sul, Av. Bento Gonçalves, 9500, CP 15051, CEP 91501-970, Porto Alegre, RS, Brazil
[2] Centro de Física de Materiales CFM/MPC (CSIC-UPV/EHU), Paseo Manuel de Lardizabal 5, E-20018 Donostia-San Sebastián, Spain
[3] Donostia International Physics Center (DIPC), Paseo Manuel de Lardizabal 4, E-20018 Donostia-San Sebastián, Spain and Centro de Física de Materiales CFM/MPC (CSIC-UPV/EHU), Paseo Manuel de Lardizabal 5, E-20018 Donostia-San Sebastián, Spain
[4] Institut des Sciences Moléculaires d'Orsay, ISMO, Unité de Recherches CNRS-Université Paris-Sud UMR 8214, Bâtiment 351, Université Paris-Sud, F-91405 Orsay Cedex, France
[5] División Colisiones Atómicas, Instituto Balseiro and Centro Atómico Bariloche, Comisión Nacional de Energía Atómica, 8400 San Carlos de Bariloche, Argentina
[6] Department Operation Accelerator BESSY II (NP-ABS), Helmholtz-Zentrum Berlin für Materialien und Energie GmbH, Hahn-Meitner-Platz 1, D-14109 Berlin, Germany

E-mail: raul@if.ufrgs.br

Received 22 June 2017, revised 31 July 2017
Accepted for publication 4 August 2017
Published 24 August 2017

Abstract

The self-consistent electron–ion potential $V(r)$ is calculated for H^+ ions in an electron gas system as a function of the projectile energy to model the electronic stopping power for conduction-band electrons. The results show different self-consistent potentials at low projectile-energies, related to different degrees of excitation of the electron cloud surrounding the intruder ion. This behavior can explain the abrupt change of velocity dependent screening-length of the potential found by the use of the extended Friedel sum rule and the possible breakdown of the standard free electron gas model for the electronic stopping at low projectile energies. A dynamical interpolation of $V(r)$ is proposed and used to calculate the stopping power for H^+ interacting with the valence electrons of Al. The results are in good agreement with the TDDFT benchmark calculations as well as with experimental data.

Keywords: energy loss, stopping power, electron gas

(Some figures may appear in colour only in the online journal)

1. Introduction

The slowing down of charged particles in dense media is a subject of intensive investigations since it plays an important role in different areas of knowledge from fundamental to applied physics, materials science and medicine. It has been investigated for many years [1–3] but still there are open questions and issues to be understood [4, 5]. Nowadays, the most appealing application of the stopping power of particles in liquid and solids is in dosimetry [6] for cancer treatment [7]. This demands a better knowledge of the energy loss processes in matter and more accurate stopping power values.

The electronic energy loss of charged particles in matter is dominated by electronic ionization and excitation of the medium. These processes are important at high projectile-energies as well as at low velocities in case of conducting materials and can be described by different models and approaches [4, 5]. Particularly the energy loss to conduction

electrons in a solid has been successfully modeled by a degenerate electron gas system [4, 5, 8–17] although the breakdown of the free electron gas (FEG) concept has been recently reported [18].

Many different calculations of the stopping power of ions in a homogeneous electron–gas system have been proposed in the literature as e.g. the linear response theory [19], first and second-order perturbation schemes [8, 20, 21], transport cross-section (TCS) approaches [11, 12, 14, 15] as well as non-perturbative quantum calculations at low [10, 13] and at even a wide range of projectile energies [22].

The central aspect of most approaches is an approximate treatment of the self-consistent electron–ion scattering potential $V(\vec{r})$. For very low projectile-velocities v the ground-state scattering potential of an external charge embedded in a Fermi gas is provided by the density functional theory (DFT) [10]. For high-energy projectiles the potential can be obtained by perturbation theory or from the Lindhard dielectric function [19]. It is a non-central potential and has axial symmetry around the ion velocity direction. The general form of $V(\vec{r})$ as a function of ion velocity is still an issue. Numerous publications just use a Yukawa-type potential (atomic units and non-relativistic expressions are used throughout this paper if not explicitly stated otherwise):

$$V(r) = -Z\frac{\mathrm{e}^{-\alpha r}}{r}, \tag{1}$$

where Z is the atomic number of the projectile and α^{-1} is a velocity-dependent screening length [5, 11, 14, 16, 23], because of its simplicity and affinity with the Thomas–Fermi solution at $v = 0$. At high projectile-energies the use of Yukawa potential in connection with the extended Friedel sum rule (FSR) for finite velocities [15] gives $\alpha = \omega_\mathrm{p}/v$ (ω_p is the plasmon frequency, related to the Fermi velocity v_F of the electron gas straightforwardly). This is consistent with the spherical average of the scattering potential calculated by perturbation theory.

In this work, we calculate the electron–ion potential self-consistently as a function of projectile energy and charge state. This procedure will shed some light on three issues found in stopping calculations: (i) What is the best electron–ion potential? (ii) How large is the effect of different degrees of excitation of the electron cloud surrounding the intruder ion? (iii) What does happen at the transition from $v < v_\mathrm{F}$ to $v > v_\mathrm{F}$? Finally the scattering potential $V(r)$ is used to calculate the stopping power for H^+ on Al using the recent formula developed in [24], which is based on the force related to the induced electron density and not on the momentum-transfer rate of the projectile. The results are compared to standard TCS [14, 15] as well as to time-dependent density functional theory (TDDFT) [22, 25] calculations.

2. Theoretical procedure

Assuming a central potential $V(r)$ for the interaction between the electrons from the medium and the projectile, the induced density $n_\mathrm{ind}(\vec{r})$ can be calculated from the partial-wave expansion of the stationary wave function for the electron-projectile collision [26],

$$\psi_{\vec{k}}(\vec{r}) = 4\pi\sum_{\ell,m} i^\ell \mathrm{e}^{\mathrm{i}\delta_\ell}\mathcal{R}_{k,\ell}(r)Y_{\ell,m}(\hat{r})Y^*_{\ell,m}(\hat{k}), \tag{2}$$

in the reference frame where the projectile is at rest. Then $\vec{k}$ corresponds to the incident electron momentum, and $\mathcal{R}_{k,\ell}(r)$ is the corresponding radial continuum wave function with angular-momentum quantum-number ℓ. The radial wave function is obtained from the radial Schrödinger equation

$$\left(-\frac{\mathrm{d}^2}{\mathrm{d}r^2} + \left(2V(r) + \frac{\ell(\ell+1)}{r^2}\right) - k^2\right)r\mathcal{R}_{k,\ell}(r) = 0. \tag{3}$$

The spherical harmonics $Y_{\ell,m}$ from equation (2) are functions of $\hat{r}$ and $\hat{k}$, directions of $\vec{r}$ and $\vec{k}$ respectively, and depend on the azimuthal quantum-number m ($|m| \leqslant \ell$). The phase-shifts δ_ℓ, obtained from the asymptotic limit ($r \to \infty$) of the radial wave function as

$$\mathcal{R}_{k,\ell}(r) \to \frac{1}{r}\sin\left(kr - \ell\frac{\pi}{2} + \delta_\ell\right), \tag{4}$$

depend on the scattering energy or, more accurately, on the asymptotic electron momentum k. As a physical boundary condition, we require charge-neutrality, i.e., the total charge of the system electron gas plus intruder is zero. The induced electron-density then reads [17]

$$n_\mathrm{ind}(\vec{r}) = \frac{2}{(2\pi)^3}\int_\mathrm{DFS}(|\psi_{\vec{k}}|^2 - 1)\mathrm{d}^3k, \tag{5}$$

where the $\vec{k}$ integration is performed over the displaced Fermi sphere [15, 17, 27], the target Fermi sphere in the reference frame where the projectile is at rest. The induced density from equation (5) can be then used to calculate the total point-symmetric electron–ion scattering potential according to

$$V(r) = -\frac{Z}{r} + \int\frac{\langle n_\mathrm{ind}(\vec{r}')\rangle + \rho_\mathrm{b}(\vec{r}')}{|\vec{r} - \vec{r}'|}\mathrm{d}^3r' + \mathcal{V}_\mathrm{xc}(\vec{r}), \tag{6}$$

where $\langle ...\rangle$ stands for spherical averaging. $\mathcal{V}_\mathrm{xc}(\vec{r})$ is the exchange/correlation potential from [28] and implemented as in [13]. Bound states, if any, are calculated by solving the radial Schrödinger equation equation (3) for negative energies or imaginary values of k. They are included in equation (6) through the bound-state density (ρ_b), which is normalized to the number of bound electrons n_b. For the present case only 1s bound electrons are considered and $n_\mathrm{b} = 0$, 1 or 2 are input parameters. Equations (3)–(6) are solved self consistently using the method described in [29], which provides a faster convergence. The results for a static proton and $n_\mathrm{b} = 2$ agree with previous calculations [10, 29].

According to the Levinson theorem [30] the number of available bound states $n_\mathrm{b}^\mathrm{avail}$ of $V(r)$ can be obtained from phase-shifts at vanishing scattering energies ($\delta_\ell(0)$) as

$$n_\mathrm{b}^\mathrm{avail} = \frac{2}{\pi}\sum_{\ell=0}^{\infty}(2\ell+1)\delta_\ell(0), \tag{7}$$

which is not necessarily equal to the number of bound states n_b. The neutralization condition

$$Z - n_b = \int d^3r\, n_{ind}(\vec{r}) \tag{8}$$

and equation (5) lead to the extended FSR as derived recently in [17], and reads [15]

$$Z - n_b = \frac{2}{\pi}\sum_{\ell=0}^{\infty}(2\ell + 1)G_\ell(v, v_F) \tag{9}$$

with

$$G_\ell(v, v_F) = \int_{|v-v_F|}^{v+v_F} dk\left(\frac{k^2 + v_F^2 - v^2}{4k^2v}\right)\delta_\ell(k) - \Theta(v_F - v)\delta_\ell(0), \tag{10}$$

where $\Theta(x)$ denotes the step function. According to the Levinson theorem equation (7) the last term of equation (10) cancels out with n_b for $v < v_F$ and for the case where all available bound states are occupied ($n_b = n_b^{avail}$). The potential used to start the self-consistent-field (SCF) iteration was selected to fulfill the condition equation (9).

The electronic stopping power can be calculated from the induced force $\vec{F}_{ind}$ at the projectile ($\vec{r} = 0$) or induced density as

$$\frac{dE}{dz} = -\frac{1}{v}\vec{F}_{ind}\cdot\vec{v} = -Z\left[\int\frac{\partial}{\partial z}\left(\frac{n_{ind}(\vec{r}\,')}{|\vec{r} - \vec{r}\,'|}\right)d^3r'\right]_{\vec{r}=0}, \tag{11}$$

for a bare ion with charge Z. Equation (11) can be written in terms of the phase-shifts from the scattering potential $V(r)$ as demonstrated recently in [24] and reads

$$\frac{dE}{dz} = \frac{Z}{8\pi v^2}\int_{|v_F-v|}^{v_F+v}\frac{dk}{k} \times (2k^2(v_F^2 + v^2) - k^4 - (v_F^2 - v^2)^2) \times \sum_{\ell=0}^{\infty}\sin(2(\delta_\ell(k) - \delta_{\ell+1}(k))), \tag{12}$$

which is notably different from the TCS approach [5, 31, 32] and gives the correct asymptotic behavior at high velocities [24]. This formula was derived by calculating the electrostatic force due to the full induced density, which has cylindrical symmetry. A partial wave analysis has been used for the electron–ion scattering described by a pre-determined central potential, e.g. from equation (1). The drawback of the standard formula for the electronic energy loss based on the transport or momentum transfer cross-section is the use of a central potential to describe the electron–ion scattering at high projectile energies. This leads to a slow convergence of the results to the expected Bethe formula. Both approaches should yield identical results, however, if the exact (non-central) interaction potential is used. The derivation described above, similar to [12], and specifically given by equation (12), may be termed induced-density approach (IDA) and will be investigated here for low projectile energies and compared to the traditional approach and to benchmark calculations.

For the sake of comparison, we will also show TDDFT calculations [22, 25, 33] of the electronic stopping power for spherical jellium clusters. Except for slight improvements of the precision, the methodology is the one already used in [22, 25] and therefore it is only briefly summarized here. The ground state of the jellium clusters was obtained using DFT [34] with a local-density approximation exchange and correlation potential [28]. Effective electronic densities of the clusters were defined by $r_s = 1.5$, 1.8, and 2.07. For the interaction dynamics, the ground-state Kohn–Sham orbitals were propagated in time using the so-called wave packet propagation method [25, 35–37] and the time-dependent density was obtained. This allowed us to calculate the Coulomb force experienced by the projectile as a function of its position. The average energy loss ΔE was calculated by integrating the force along the whole trajectory of the proton: $\Delta E = -v\int F_z(t)dt$. The stopping power is then calculated as the average energy loss per unit path length inside the cluster, i.e. $S = \Delta E/2R_{cl}$, where R_{cl} is the cluster radius. In principle, this describes an energy loss treatment based on the induced density related to time-dependent DFT for a finite cluster, whereas the current model is based on the self-consistent electrostatic continuum-electron field in an infinite electron–gas solid.

3. Discussion

Before showing some numerical results we notice that when solving the SCF (equation (6)), one has the option of modifying the number of bound electrons attached to the projectile, n_b, to represent different possible charge states. The ground state of the projectile corresponds to the case where n_b satisfies Levinson's theorem ($n_b = n_b^{avail}$) as long as the available states exist energetically below the Fermi level; the corresponding potential in this case is called the ground-state potential. Otherwise said, the self-consistent procedure allows us to obtain different values of the continuum induced density (and thus of the scattering potential) depending on the population of the bound states, which is imposed ad-hoc at the beginning of the calculation. In each case, the total screening charge induced in the continuum remains equal to $-(Z - n_b)$. By using lower values of n_b we can represent ions with various charge states, $q = Z - n_b$, in particular when $n_b = 0$ we obtain fully stripped ions. The corresponding potentials where $n_b \neq n_b^{avail}$ will be called excited potentials.

Figure 1 shows the self-consistent solution for the total spherical electron–ion scattering potential from equation (6) for 100 keV H^+ in an FEG system corresponding to the Al valence electrons (electron radius $r_s = 2.07$). The solution is very close to a Yukawa potential from equation (1) with inverse screening length $\alpha = 0.29$. This value is the same as the one given by the extended FSR for the Yukawa potential. The same holds true for other projectile velocities above the Fermi velocity ($v > v_F$). In addition, for $v \to 0$ the solution contains the Friedel oscillations [38], but their amplitude is very small and they are of minor importance for the electron scattering at the present energies. Therefore, for H^+ ions in Al

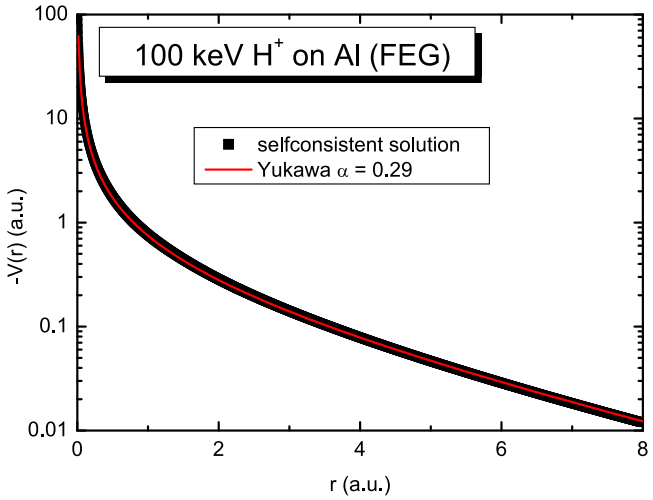

Figure 1. Self-consistent effective $V(r)$ for 100 keV H^+ ions in a FEG system with electron radius $r_s = 2.07$ corresponding to Al valence-electron density of 1.81×10^{23} cm^{-3}. The square symbols correspond to the present calculations. The red solid-line represents the Yukawa potential from equation (1) with inverse screening length $\alpha = 0.29$.

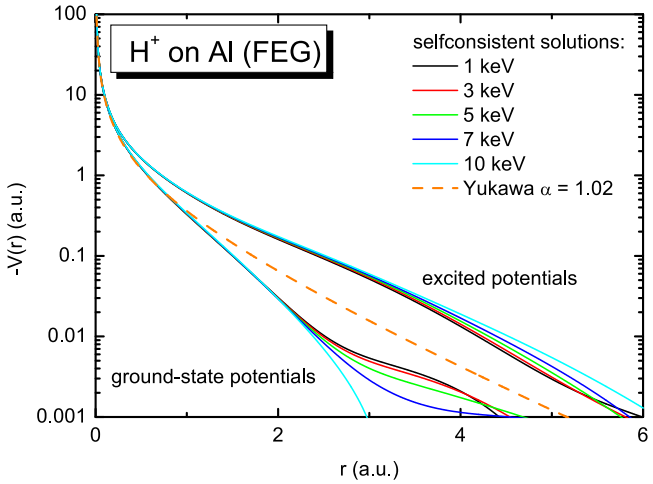

Figure 2. The same as in figure 1 for lower velocities ($v < v_F$). Two solutions for each projectile energy are shown.

the Yukawa potential is a nearly perfect spherical approximation of the self-consistent potential, to be used in stopping power models based on binary collisions between the valence electrons and the projectile. In addition the corresponding screening length is well described by the extended FSR.

The self-consistent scattering potentials for 1–10 keV H^+ ions on the Al valence electrons are displayed in figure 2. These projectile energies correspond to $v < v_F$ and show the possibility of multiple solutions according to the value of $n_b = 0$ and 2. The solution where the projectile is more strongly screened (i.e. with smallest value of $|V(r)|$) is well represented by a Yukawa potential with inverse screening length $\alpha = 1.02$, which deviates from $\alpha_0 = \alpha(v = 0) = 1.24$ given by the static FSR because of exchange/correlation effects. This solution corresponds to $n_b = 2$ and thus to a stable H^- embedded in the electron gas. The other one, denoted by *excited potential* (V_{exc}), leads to the upper group of curves in figure 2 and has

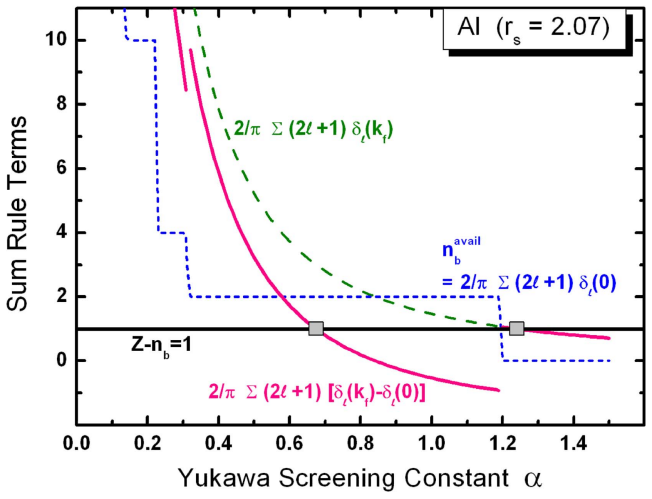

Figure 3. Different sum-rule terms are displayed for an aluminum target as function of the Yukawa-screening constant. The green long-dashed curve is proportional to the right-hand side of equation (9) for $v > v_F$. The blue short-dashed curve displays the Levinson theorem equation (7). The pink solid curve displays the right-hand side of equation (9) for $v < v_F$ and the constant value of 1 corresponds to the left-hand side.

$n_b = 0$. It is pointed out that for $r_s < 2$ where there are no bound-states ($n_b = 0$) other solutions can also appear for different starting conditions of the SCF iteration.

The existence of extra solutions can also be extracted from the extended FSR for different n_b as defined by equations (9) and (10). However, even for a fixed value of n_b (e.g. $n_b = 0$) equations (9) and (10) can give different solutions as explained in figure 3. Under the assumption of a Yukawa-type projectile potential we may use the extended FSR given by equation (9) for estimating the number of possible SCF solutions as well as the corresponding screening constants α. For fast protons, the right-hand side of equation (9) is monotonically decreasing (see dashed green curve) and thus there is only a single value of α that solves the equation for a fixed value of n_b ($n_b = 0$ in the present case). For slow protons, the right-hand side of equation (9) shows kinks as a function of α (solid pink curve). These kinks are related to the number of unoccupied bound states as defined by equation (7) for $n_b = 0$. Generally this means, multiple solutions are possible and we find $\alpha = 0.674$, 1.24 for Al (indicated by the two square symbols in the figure, where solid pink curve segments cross the black line). The first solution corresponds to the excited potential and the latter solution represents the ground state. It is emphasized that our Yukawa fits to the numerical SCF potential are close to these α-values and the deviations are due to exchange/correlation effects.

Figure 4 shows the self-consistent scattering potentials for different velocities close to v_F. As can be observed the potentials at projectile energies $\gtrsim$30 keV ($v > v_F$) are single-valued (a numerical search for other solutions with $n_b = 0$ failed in this velocity regime). These high-velocity SCF solutions merge with the excited-state potentials at lower energies (see the dashed curve). Therefore, the transition

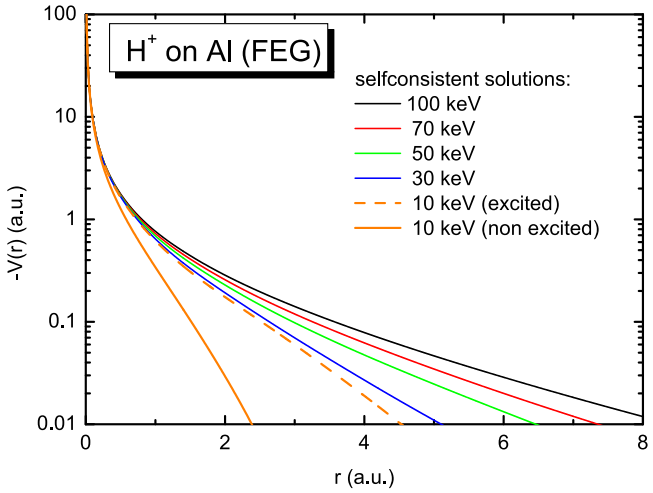

Figure 4. The same as in figure 1 for projectile velocities around v_F. Note for $E \geqslant 30$ keV all curves correspond to excited potentials.

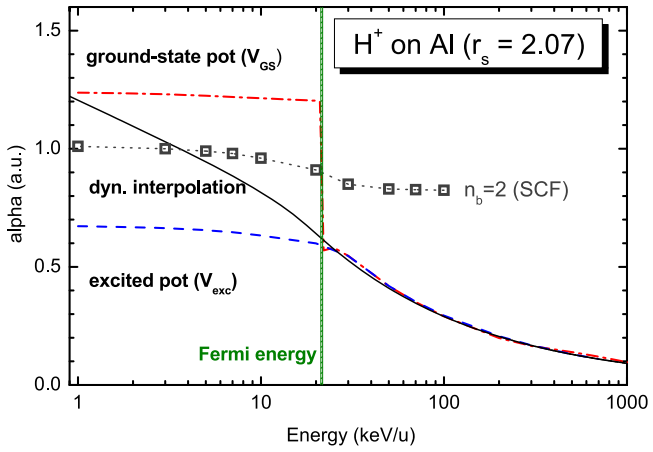

Figure 5. Inverse of the screening length α as a function of the projectile energy calculated using the extended Friedel sum from [15] and Yukawa potential from equation (1). For $v < v_F$ different values of α are found for ground-state potential (red dot-dashed line) and excited potential (blue dashed line). The continuous solid line stands for the results obtained via dynamical interpolation (equation (13)). The symbols correspond to Yukawa fits to the our numerical SCF results for $n_b = 2$.

$v < v_F$ to $v > v_F$ is smooth if one considers only these excited potentials. On the other hand, the transition is abrupt for non-excited potentials (-ground-state potential V_{GS}).

This discontinuity can also be observed in figure 5, where the inverse of the screening length α is obtained from the extended FSR (equation (9)) using the Yukawa potential from equation (1). The two solutions for $v < v_F$ are denoted by V_{GS} and V_{exc} . The actual scattering potential is expected to be a mixture of ground-state (dash-dotted line) and excited (dashed line) potentials. However, the ground-state solution should prevail at $v = 0$. The solid line in figure 5 corresponds to such a dynamical interpolation

$$\alpha(v)^{-4} = \alpha_0^{-4} + \left(\frac{\omega_p}{v}\right)^{-4}, \qquad (13)$$

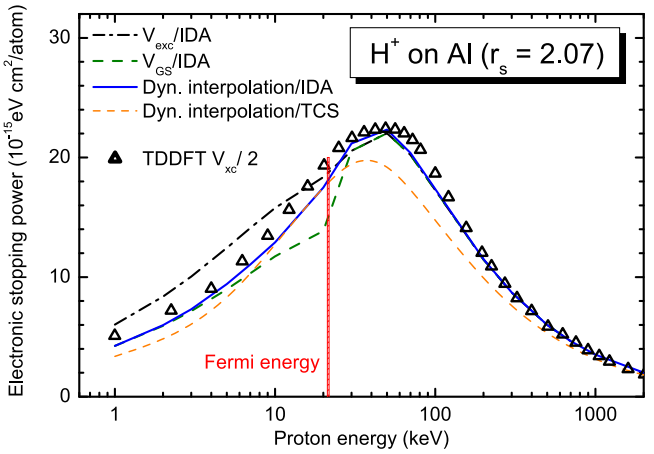

Figure 6. Electronic stopping power for H^+ ions on Al valence electrons as a function of the projectile energy for different screening parameter α from figure 5.

which can be used to calculate a more realistic stopping power involving a weighted superposition of potentials. Here α_0 is the α value for the ground-state potential at $v = 0$ using the static FSR and ω_p/v is the solution at high-projectile energies.

It is pointed out that the transition around v_F is not discontinuous for a fixed n_b in the SCF calculations (see symbols for $n_b = 2$ in figure 5). Nevertheless the cases $n_b \neq 0$ do not prevail at high projectile energies. Therefore, the discontinuity found in the FSR method arises from the link between the ground-state solutions (valid at low energies) with the excited solutions (valid at high energies).

The three FSR results of α from figure 5 were used to calculate the electronic stopping power according to equation (12). The corresponding stopping powers for H^+ ions on Al valence electrons as a function of the energy are displayed in figure 6 in comparison with TDDFT calculations (triangle) that can be considered as a benchmark. These calculations were performed similarly to [22] but the value of the exchange-correlation (XC) potential has been reduced by a factor of 2 to allow for a more suitable comparison with the extended FSR—IDA model, which is based on the use of the Yukawa potential. The XC potential cannot be totally removed because it is a key factor in the energy stabilization of the DFT jellium cluster, unless additional procedures are used (see for example [39]). We have checked that the electronic density profile of the cluster does not vary significantly with the reduction of the XC potential and hence all differences in the stopping are due to the dynamical process itself.

At high energies a good agreement is expected since all calculations converge to the Bethe formula. For low energies (at $v \sim v_F$) a discontinuity is observed for the IDA calculations using ground-state potentials V_{GS} (see green long-dashed line). However, as already observed in figures 4 and 5 the transition using excited potential V_{exc} is smooth (as shown by the dash-dotted line). At low energies the present calculations using V_{GS} and V_{exc} under and overestimate the results from TDDFT, respectively. This indicates that actual ion–electron potential should be in between. The dynamical

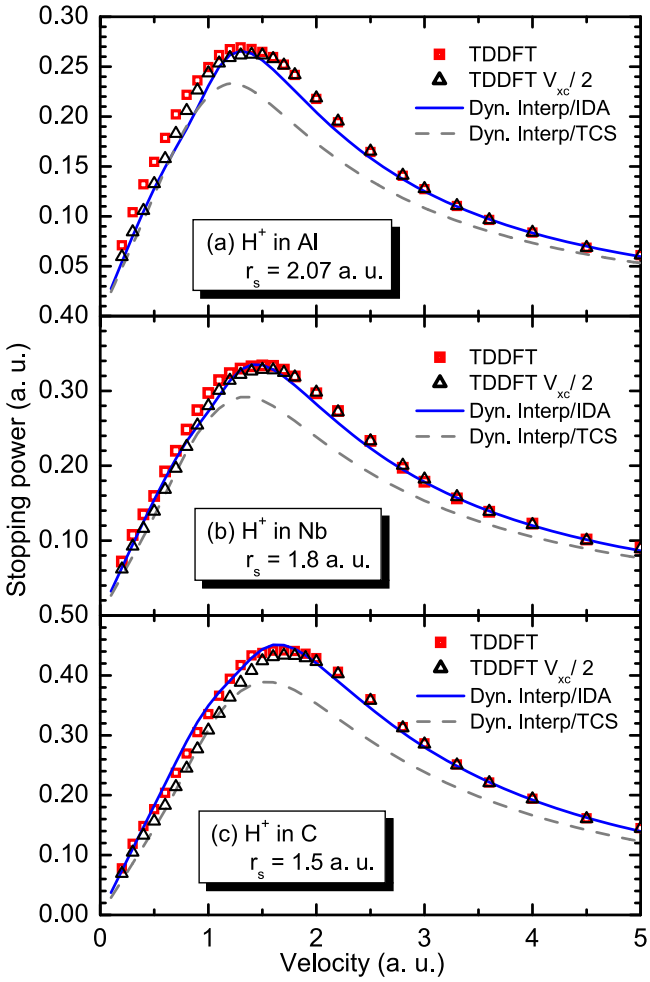

Figure 7. Stopping power results of a proton moving inside clusters of Al (a), Nb (b) and C (c) as a function of its velocity. The symbols stand for TDDFT (red squares) and TDDFT with reduced $\mathcal{V}_{xc}$ (triangles) evaluations from a cluster with 556 electrons. The lines stand for the dynamical interpolation results using IDA (blue) and TCS (dashed gray).

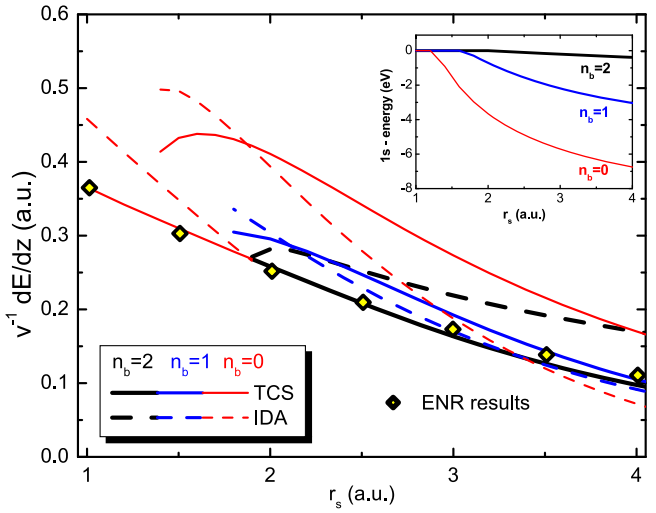

Figure 8. Self-consistent (DFT) calculations for the stopping coefficient in the limit $v \to 0$ using the TCS (solid line) and IDA (dashed line) approaches for a fixed n_b. Inset shows the energy of the 1s bound-state as a function of r_s. Previous DFT results from Echenique, Nieminen and Ritchie ENR [10] are shown by symbols.

interpolation from equation (13) (see solid line) seems to better reproduce the trend given by TDDFT calculations. Figure 6 also shows the calculations using the TCS [5] with Yukawa potential and α from the dynamical interpolation (13) (orange short-dashed line). As expected [24] it reaches the high-energy stopping solution only at very high energies and cannot reproduce TDDFT values around the maximum of the stopping power.

The remaining differences between our new results (Dyn. Interpolation/IDA) and the TDDFT at low energies can be related either to the XC effects, considered partially only in the TDDFT or to intrinsic inaccuracies of the IDA formula at $v \to 0$. The importance of XC effects is shown in figure 7 for the stopping power as a function of ion velocity for protons in different electron gas densities. We have considered three valence electrons for Al, with $r_s = 2.07$ au, five for Nb, with $r_s = 1.8$ au and four for C, with $r_s = 1.5$ au.. Here we replaced the α_0 from equation (13) by our Yukawa fits (up to $r = 1$) to the numerical SCF potential at $v = 0$,

$$\alpha_0^{\mathrm{DFT}} = \sqrt{\frac{2.44}{r_s + 2.75r_s^2 - 1.14r_s^3 + 1.73r_s^4}} + 0.754, \quad (14)$$

that have been extracted from calculations for different r_s values. This result contains exchange/correlation effects and converges to the α_0 obtained from the Born approximation for $r_s \to 0$ [15]. In all studied cases, for larger velocities (or more perturbative conditions), the dynamical interpolation/IDA shows an improved agreement to the TDDFT results if compared to the TCS values. XC effects are significant only below the stopping-power maximum and reach typically 20%. A maximum reduction of the stopping power by about 40% (determined from the TDDFT results extrapolated to $\mathcal{V}_{xc} = 0$) is found for the Al target at the speed $v = 0.4$ au. Considering that the IDA and TCS results in figure 7 account both for XC effects, the TDDFT benchmark results do favor the IDA method in some ranges of energy and the TCS method for other cases.

As a matter of fact for $v \to 0$ [13] the TCS approach should be the correct one to describe the stopping ion in a FEG system as long as bound-state polarization is of minor importance. For the present cases both models give similar results for the stopping at low projectile velocities. However, this is not always the true and the IDA approach can yield inaccurate stopping values at $v \to 0$ because of the use of a central potential $V(r)$ [13]. In fact [13] shows that the dipolar part of the potential contributes to a term proportional to v^2 for the TCS method whereas it contributes linearly for the IDA approach.

Figure 8 presents the results for stopping coefficient $Q = v^{-1}\mathrm{d}E/\mathrm{d}z$ as a function of r_s . Here our SCF method is performed for $v = 0$ and the Q values are obtained by the TCS and IDA formulas using the self-consistent potentials for

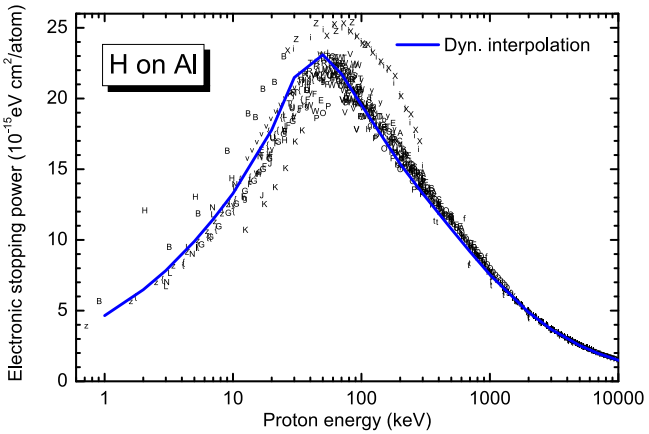

Figure 9. Electronic stopping power for H^+ ions on Al as a function of the projectile energy. The experimental results (individual letters represent specific measurements) are taken from the stopping collection of Helmut Paul [43].

different n_b. The TCS results for V_{GS} agree with recent results from Montanari and Miraglia [14]. For $n_b \neq 0$ the IDA formula from equation (12) has to be replaced by the one described in the appendix of [24] to account for the wake force on the bound electrons as described in equations A(21) and A(22), where $\Phi'(r)$ stands for the force generated by the bound electrons.

As can be observed there are also different solutions even for a fixed value of $n_b = 0$. The energy of the 1s bound-state as a function of r_s is also displayed in this figure (see the inset) and shows the values of r_s where there is no bound-state available (zero binding energy). Both methods give similar results only for r_s values around 2 and the IDA approach can even yield negative Q values for $r_s \gg 4$. Another interesting feature of this figure is the strong dependence of Q on the number of populated bound-states. The possibility of different values of n_b is generally ignored in the comparison of DFT calculations with ion-stopping experimental data at very low ion velocities [18].

Finally, the results for the electronic stopping power of H^+ ions on Al valence electrons from figure 7 (top panel) are used to calculate the total electronic stopping power by adding the contribution of the inner-shells as calculated by the CasP program [40, 41] and by neglecting a possible H^0 fraction inside the solid. Note, however, that the formation of H^0 may be significant in front of the surface [42]. Figure 9 shows a comparison with all available experimental data obtained from the stopping power collection of Paul [43]. Our calculation based on equations (13) and (14) (solid curve) describes the experimental data very well for the whole energy range.

4. Conclusions

In this work, we investigated the electronic stopping power for H^+ projectiles in the valence electrons of solids, with a focus on Al. The self-consistent potential for the scattering of valence-electrons at the projectile was analyzed and compared to extended FSR calculations. We have shown that the spherical average of this potential is a function that is very close to a Yukawa potential for $v > v_F$. This agrees with predictions based on perturbation theory. The same holds true for $v < v_F$ but other self-consistent solutions appear as well. These extra solutions correspond to excited potentials and can also be obtained by the extended FSR after relaxing the condition imposed by the use of the Levinson theorem. The transition from $v < v_F$ to $v > v_F$ becomes smooth as long as excited potentials are used. However, at very low energies the ground-state potential should describe the interaction correctly. Thus, a dynamical interpolation has been proposed yielding a good agreement with TDDFT benchmark calculations as well as with experimental data after adding the contribution of the inner-shells from the CasP program.

Acknowledgments

We are indebted to the Brazilian agencies CAPES, CNPq and FAPERGS for the partial support of this research project. One of the authors (PLG) acknowledges funding by the Alexander-von-Humboldt foundation. NEK and RDM acknowledge financial support by the Basque Departamento de Educación, Universidades e Investigación, the University of the Basque Country UPV/EHU (Grant No. IT-756-13) and the Spanish Ministerio de Economía y Competitividad (Grants FIS2013-48286-C02-02-P and FIS2016-76471-P).

References

[1] Thomson S J 1912 *Phil. Mag.* 6 **23** 449–57
[2] Bohr N 1913 *Phil. Mag.* **25** 10–31
[3] Bethe H A 1930 *Ann. Phys.* **397** 325–400
[4] Sigmund P 2006 *Particle Penetration and Radiation Effects* (vol 151) vol 1 1st edn (Berlin: Springer)
[5] Sigmund P 2014 *Particle Penetration and Radiation Effects* (vol 179) vol 2 1st edn (Berlin: Springer)
[6] McParland B J 2014 *Medical Radiation Dosimetry: Theory of Charged Particle Collision Energy Loss* (London: Springer)
[7] Newhauser W D and Zhang R 2015 *Phys. Med. Biol.* **60** R155
[8] Ferrell T L and Ritchie R H 1977 *Phys. Rev.* B **16** 115–23
[9] Echenique P M, Nieminen R M, Ashley J C and Ritchie R H 1986 *Phys. Rev.* A **33** 897–904
[10] Echenique P M, Nieminen R M and Ritchie R H 1981 *Solid State Commun.* **37** 779–81
[11] de Ferrariis L and Arista N R 1984 *Phys. Rev.* A **29** 2145–59
[12] Zaremba E, Arnau A and Echenique P 1995 *Nucl. Instrum. Methods Phys. Res.* B **96** 619–25
[13] Salin A, Arnau A, Echenique P M and Zaremba E 1999 *Phys. Rev.* B **59** 2537–48
[14] Montanari C C and Miraglia J E 2017 *Phys. Rev.* A **96** 012707
[15] Lifschitz A F and Arista N R 1998 *Phys. Rev.* A **57** 200–7
[16] Nagy I and Bergara A 1996 *Nucl. Instrum. Methods Phys. Res.* B **115** 58–61
[17] Nersisyan H B, Fernandez-Varea J M and Arista N R 2015 *Nucl. Instrum. Methods Phys. Res.* B **354** 167–71
[18] Roth D *et al* 2017 *Phys. Rev. Lett.* **118** 103401
[19] Lindhard J and Winther A 1964 *Mat. Fys. Medd. Dan. Vid. Selsk* **34** 1

[20] Pitarke J M, Ritchie R H, Echenique P M and Zaremba E 1993 *Europhys. Lett.* **24** 613–9
[21] Pitarke J M, Ritchie R H and Echenique P M 1995 *Phys. Rev.* B **52** 13883–902
[22] Quijada M, Borisov A G, Nagy I, Díez-Muiño R and Echenique P M 2007 *Phys. Rev.* A **75** 042902
[23] Sigmund P and Schinner A 2000 *Eur. Phys. J.* D **12** 425–34
[24] Grande P L 2016 *Phys. Rev.* A **94** 042704
[25] Koval N E, Sánchez-Portal D, Borisov A G and Díez-Muiño R 2013 *Nucl. Instrum. Methods Phys. Res.* B **317** 56–60
[26] Messiah A 1963 *Quantum Mechanics* vol 2 (New York: Dover)
[27] Bonderup E 1981 Interaction of charged particles with matter. Institute of Physics, Aarhus, www.phys.au.dk/~ahs/EBnotes.htm
[28] Gunnarson O and Lundqvist B 1976 *Phys. Rev.* B **13** 4274–98
[29] Jena P and Singwi K S 1978 *Phys. Rev.* B **17** 3518–24
[30] Wellner M 1964 *Am. J. Phys.* **32** 787–9
[31] Finnemann J 1968 En redegørelse for resultaterne af beregninger over spredning af elektroner med lav energi på afskærmede Coulombfelter *Masteras Thesis* Aarhus University
[32] Briggs J S and Pathak A P 1973 *J. Phys. C: Solid State Phys.* **6** L153–7
[33] Pruneda J M, Sánchez-Portal D, Arnau A, Juaristi J I and Artacho E 2007 *Phys. Rev. Lett.* **99** 235501
[34] Hohenberg P and Kohn W 1964 *Phys. Rev.* **136** B864–71
[35] Borisov A G, Juaristi J I, Díez-Muiño R, Sánchez-Portal D and Echenique P M 2006 *Phys. Rev.* A **73** 012901
[36] Borisov A G, Gauyacq J P and Shabanov S V 2001 *Surf. Sci.* **487** 243–57
[37] Chulkov E V, Borisov A G, Gauyacq J P, Sánchez-Portal D, Silkin V M, Zhukov V P and Echenique P M 2006 *Chem. Rev.* **106** 4160–206
[38] Gabovich A M, Il'chenko L G, Pashitski E A and Romanov Y A 1978 *Sov. Phys.—JETP* **48** 124–31
[39] Perdew J P, Tran H Q and Smith E D 1990 *Phys. Rev.* B **42** 11627–36
[40] Grande P L and Schiwietz G 2006 Convolution Approximation for Swift Particles (CasP) program, free http://casp-program.org
[41] Schiwietz G and Grande P L 2011 *Phys. Rev.* A **84** 052703
[42] Winter H 1996 *J. Phys.: Condens. Matter* **8** 10149–83
[43] Paul H 2015 Stopping power of matter for ions graphs, data, comments and programs https://nds.iaea.org/stopping/